Journal Name

ARTICLE

Oligothiophene/graphene supramolecular ensembles managing light induced processes: Preparation, characterization, and femtosecond transient absorption studies leading to charge-separation

Received 00th January 20xx,
Accepted 00th January 20xx

DOI: 10.1039/x0xx00000x

www.rsc.org/

A. Stergiou,[a] H. B. Gobeze,[b] I. D. Petsalakis,[a] S. Zhao,[c] H. Shinohara,[c] F. D'Souza[b,*] and N. Tagmatarchis[a,*]

Advances in organic synthetic chemistry combined with the exceptional electronic properties of carbon allotropes, particularly graphene, is the basis to design and fabricate novel electron donor-acceptor ensembles with desired properties for technological applications. Thiophene-based materials, mainly thiophene-containing polymers, are known for their notable electronic properties. In this frame moving from polymer to oligomer forms, new fundamental information would help to the better understanding of their electrochemical and photophysical properties. Furthermore, a successful combination of their electronic properties with those of graphene is a challenging goal. In this work two oligothiophene compounds consists of three and nine thiophene-rings, abbreviated as **3T** and **9T**, respectively, were synthesized and noncovalently associated with liquid phase exfoliated few-layered graphene sheets (abbreviated as **eG**), forming donor-acceptor **3T/eG** and **9T/eG** nanoensembes. Markedly, intra-ensemble electronic interactions between the two components in the ground and excited states were evaluated with the aid of UV-Vis and photoluminescence spectroscopy. Furthermore, redox assays revealed an one-electron oxidation of **3T** accompanied by one-electron reduction due to **eG** in **3T/eG**, while two reversible one-electron oxidations of **9T** accompanied by one-electron reduction of **eG** **9T/eG**. The electrochemical band gap for **3T/eG** and **9T/eG** ensembles were calculated and verified that the negative free-energy change for the charge-separated state of **3T/eG** and **9T/eG** via the singlet excited state of **3T** and **9T** respectively, were thermodynamically favorable. Finally, results of transient pump-probe spectroscopic studies at the femtosecond time scale were supportive of charge transfer type interactions in the **3T/eG** and **9T/eG** ensembles. The estimated rates for intra-ensemble charge separation were found to be 9.52 x 10^{9} s^{-1} and 2.2 x 10^{11} s^{-1}, respectively, for **3T/eG** and **9T/eG** in THF, revealing moderate to ultrafast photoinduced events in the oligothiophene/graphene supramolecular ensembles.

Introduction

The rise of graphite exfoliation pumping up graphene's chemistry brings significant impact towards the preparation of novel hybrid materials, combining the exceptional mechanical and electronic properties of single and few-layered graphene sheets[1] with those of photoinduced electron and/or energy transfer from organic chromophores interacting with the carbon nanostructure.[2] In this frame, research efforts worldwide aim towards the preparation of diverse graphene-based nanohybrids fabricated by covalent or non-covalent synthetic methodologies[3] and the evaluation of their electrochemical and photophysical properties in solution,[4] thereby, overtaking insolubility issues, which is the major drawback together with the need of suitable exfoliating routes of graphite.

Applications including charge transfer processes demand both defect free, single- and/or few-layer graphene sheets and robust chemical procedures for the chemical or supramolecular grafting of the desired organic moieties onto the sp^2-honeycomb lattice of graphene. Covalent chemistry of graphene leads to strong interactions between the organic material and the graphitic skeleton, however, introduces defects at the anchoring sites, thus, acting as insulators.[2] Nevertheless, free and Pd-metallated tetraphenylporphyrins,[5] phthalocyanines[6] and ruthenium bipyridyl complexes[7] were incorporated onto graphene, through pyrrolidine ring formation under [3+2] cycloaddition reactions. Additionally,

[a] Theoretical and Physical Chemistry Institute, National Hellenic Research Foundation, 48 Vassileos Constantinou Avenue, Athens 11635, Greece
[b] Department of Chemistry, University of North Texas, 1155 Union Circle, #305070, Denton, TX 76203-5017, USA
[c] Department of Chemistry, Nagoya University, Nagoya 464-8602, Japan
Electronic Supplementary Information (ESI) available: [NMR, MS, ATR-IR, UV-Vis spectra, CV graphs, femto- and nano-second transient absorption spectra of oligothiophenes and their ensembles with exfoliated graphene]. See DOI: 10.1039/x0xx00000x

tetrathiafulvalene units were anchored onto graphene sheets via Bingel cyclopropanation,[8] zinc-phthalocyanine derivatives via nucleophilic addition of primary amines[9] or click-chemistry conditions,[10] yielding materials with strong intrahybrid electronic interactions.

On the other hand, when supramolecular interactions are utilized to integrate organic moieties to graphene, the resulted hybrids although may suffer from the weaker π-π interactions and the subsequent release part of the organic units to the solution, the extended aromatic lattice of graphene sheets remains intact and undisrupted, as no bond formation takes place, thus allowing for ballistic transport of charges with negligible loss of energy. In this frame, tripodal graphene binders of Co(II) bis-terpyridyl complexes bearing three pyrene units,[11] dendrons of perylene bisimides,[12] porphyrins,[13-15] zinc-phthalocyanines,[14] zinc phthalocyanine-based *p*-phenylenevinylene oligomers,[16] azobenzene chromophores,[17] pyrene butanoic acid succinimidyl ester and oligo(*p*-phenylenevinylene) methyl ester[18] were incorporated for the preparation of supramolecular graphene-based nanoensembles and the stabilization of single and few-layered graphene sheets upon restacking to bulk graphite. Considering also that since non-covalent immobilization of organic molecules onto the graphene sheets usually proceeds simpler and faster than bond formation, the particular approach is therefore suitable for a first estimation of plausible electronic communication between a photo- and/or electro-active organic unit and graphene. In this regard, in a recently study, accelerated charge separation in a multi-modular tris(pyrene)-subphthalocyanine-fullerene donor-acceptor hybrid upon decorating the hybrid on graphene was reported.[19]

Thiophenes belong to the family of five-membered heterocyclic aromatic rings, with the electron-rich sulfur atom conjugated to two carbon-carbon π-bonds. It is well known that the class of oligo/polythiophenes possesses great electronic properties and thiophene-based materials are amongst the most promising candidates for applications in organic electronics.[20] Thiophene-chains/polymers were used as π-bridges, because of their significant charge carrier ability,[21] connecting electron donor and electron acceptor moieties.[22] Additionally, thiophene-based oligomers and polymers, are very popular p-type semiconductors in light-emitting diodes, field effect transistors and sensors[23] and photovoltaic cells.[24] Considering the latter, manipulation of the HOMO-LUMO gap of thiophene-based oligomers and the charge transport efficiency, together with their chemical stability, i.e. upon oxidation, is a continuous opportunity for chemists, physicists and engineers.

A great advantage of such organics is the versatility of their chemistry and their low cost as starting materials. Mainly, thiophene-based or containing materials and devices consisting of polythiophene chains with a variety of functional groups attached to the carbon atoms or even to the sulfur. Since the early 90's, the scientific interest for these materials increased the attentiveness for new synthetic routes, molecular designing and a stepwise transition from bulk materials to well-defined structures.[25] Furthermore, the stability, electronic properties, morphology and a variety of special characteristics of thiophene-based materials justify researchers to further study their fundamental properties.[25]

During the last few years, the properties of oligothiophenes as well as their potent electronic applications have created a new research field following the achievements of the corresponding huge polymer family.[26] The ease, in most cases, in oligomer synthesis and characterization provides the advantage of a well-defined structure and a material with a minimum load of impurities due to the easier purification. So far, literature is full of thiophene-based organics, most of them related to the field of materials science, physics and engineering, and their individual properties but only a few reports concerning fundamental aspects were published.[26] Almost a decade ago, electrochemical studies on oligothiophenes containing 4-8 rings, showed that the oligothiophene chain length is critical for the generation of stable radical cations (i.e. oxidation process) and affects the molecule's band gap revealing additional electronic bands within the band-gap.[27] Recently, oligothiophenes containing 1-6 rings, which were synthesized and characterized with optical microscopy and electrochemical techniques, strengthen the trend of length-dependent conductance and additionally introduced the importance of their conformers to the conducting behavior.[28]

In the field of graphene-based materials incorporating oligothiophenes, only a couple of reports concerning morphological and assembly studies, to the best of our knowledge, exist. Briefly, supramolecular hybrids consisting of epitaxial graphene and 2,5-dialkoxy-phenylene-thienylene-based oligomers were studied and the impact of the alkyl chains attached on the thiophene rings to the self-assembly efficiency of the molecule over graphene's surface was evaluated.[29] Additionally, the molecular assembly of tetrathiophenes and the impact of the morphology of CVD graphene was also reported.[30] In the aforementioned works, the oligothiophenes in the graphene-based hybrids and devices function as electron donors with interesting and promising electronic properties. Therefore, it is absolutely timely and important to prepare and study such nanoensembles, particularly, targeting the evaluation of their electrochemical and photophysical properties.

The scope of the current work includes both the fundamental study of short-chain oligothiophenes properties and the fabrication of novel oligothiophene/graphene ensembles. Herein, we report for the first time the preparation of ensembles incorporating oligothiophenes and defect-free exfoliated graphene, interacting in a non-covalent fashion via multiple π-π van der Waals forces. The newly prepared materials were fully characterized by complementary spectroscopic and microscopy techniques, while their redox and photophysical properties were also evaluated. Furthermore, this work aims to the development of new synthetic and designing routes for graphene-based donor-acceptor ensembles with potent interest in optoelectronics and photovoltaics. In addition, the fundamental information received is expected to impact the better understanding of

electron and/or energy transfer phenomena and the development of thiophene-based materials and graphene hybrids with enhanced efficiency.

Results and discussion

Stille coupling, a palladium catalyzed cross coupling reaction between organostannanes and alkyl or aryl halides, is a very popular and efficient route for polycondensations.[27] Organostannanes are stable against oxidation from air and hydrolysis from moisture and usually give excellent yields. The solvent and the ligands of the palladium catalyst affect the products and their yield.[31] Initially, we intended to synthesize the 3',4'-dihexyl-2,2':5',2''-terthiophene (abbreviated as **3T**) through a coupling reaction of 2,5-di-bromo-3,4-di-hexylthiophene and 2-tributyl-stannyl-thiophene catalyzed by $Pd(PPh_3)_4$ in refluxing dry toluene. Despite the fact that the resulting product is a simple terthiophene, without carrying any sensitive group, the yield of the reaction was mediocre, while an unknown side product was also observed. In general, under common thermal conditions the reaction suffered from mediocre to no yields. A microwave reactor was an alternative to the classic thermal method. Microwave irradiation is a powerful tool in modern organic synthesis with solid advantages, such as accelerating slow reactions or competing reactions, which fail to significantly proceed under thermal conditions, restricting side reactions and offering atom, solvent and energy economy. Hence, a Stille coupling reaction under microwave irradiation conditions for the synthesis of **3T** was developed (Scheme 1).

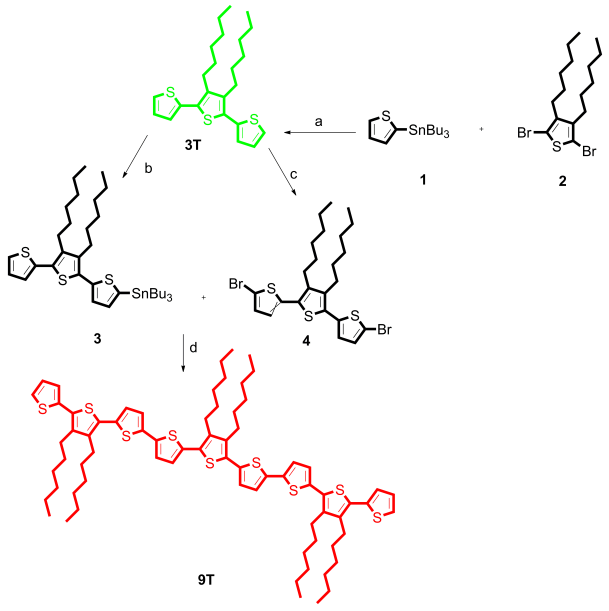

Scheme 1. Synthesis of oligothiophenes **3T** and **9T**. a: 2eq **1**, 1eq **2**, 10% $Pd(PPh_3)_4$, 10% CuI, 1eq CsF, dry DMF, 120^{0}C, MW (300 W), 1hr; b: i) 1eq **3T**, 1.2eq BuLi (2.5M in hex.), dry THF, -80 ^{0}C, 1 hr; ii) 1.2eq Bu_3SnCl, -80 ^{0}C to r.t. overnight; c: 1eq **3T**, 2.2eq NBS, dry DMF, -80 ^{0}C C to r.t. then overnight; d: 2.2eq **3**, 1eq 4, 10% $Pd(PPh_3)_4$, 10% CuI, 1eq CsF, dry DMF, 140 ^{0}C, MW (300 W), 1hr.

The success of the reaction, verifying the structure of **3T** as shown in Scheme 1, was proved by NMR spectroscopy and mass spectrometry. Briefly, in the ^{1}H NMR spectrum of **3T** (ESI, Fig. S1) three multiple peaks at the region 7.0-7.3 ppm with a 2:2:2 ratio, corresponding to the three aromatic protons of the external thiophene rings and two multiple peaks at 2.69 and 1.54 ppm referring to the four a and four b protons of the -CH_2- units attached at C-3 and C-4 of the central thiophene ring were observed. Moreover, ^{13}C NMR reveals six signals at the region of the aromatic carbons (140.45, 136.61, 130.17, 127.66, 126.20 and 125.62 ppm) corresponding to the 6 pairs of equivalent carbon atoms of the terthiophene core and six signals at the region of 10-30 ppm corresponding to the six pairs of equivalent carbons from the two hexyl chains at C-3 and C-4 (ESI, Fig. S2). Eventually, mass spectrometry revealed the M+1 ion with m/z value 417.3 amu, in full agreement with the related theoretically predicted isotopic distribution pattern, corresponding to the structure of **3T** (ESI, Fig. S3).

The hexyl-chains at C-3 and C-4 of **3T** were incorporated so as not only for achieving better solubilization in common organic solvents such as THF, dichloromethane, toluene, particularly when **3T** interacts in a non-covalent fashion with exfoliated graphene (see below), but also for better manipulating the so-formed ensemble. Furthermore, it is known that the presence of alkyl chains onto the oligothiophene backbone makes preferable the *face-on* orientation of the organic molecule onto the graphene lattice.[32] In addition, the three-ring aromatic system also offers limited rotation of the rings along the linking carbon-carbon bond leading to a planar chain sufficient for numerous π-π stacking interactions with the surface of the graphene sheets.

Our scope also includes the effect of the conjugation length to the electronic properties of the oligothiophenes and the oligothiophene/graphene ensembles. In order to proceed this study, a 9-ring thiophene (abbreviated as **9T**), which is a trimer of **3T**, was also synthesized according to Scheme 1. Briefly, **3T** was initially converted to its monostannylated derivative **3** and its di-bromo derivative **4**, which then subsequently coupled, following the same protocol for the microwave assisted synthesis of **3T**, to furnish oligothiophene **9T**. ^{1}H and ^{13}C NMR spectroscopy and mass spectrometry confirmed the structure of **9T** (ESI, Figs. S4-6). Markedly, the extended aromatic backbone of **9T** and the increased number of alkyl chains would have an impact on the intra-ensemble electronic communication, to the solubility of the ensemble and the charge transfer mechanism.

In parallel to the synthesis of **3T** and **9T**, the preparation of a capable amount of defect-free exfoliated graphene was achieved. The reported chlorosulfonic acid (CSA) mediated exfoliation process[33] considered suitable. However, since our large starting graphite flakes (>150 mesh) were poorly exfoliated to few-layered graphene under this protocol, the mechanical stirring was replaced with a bath sonicator for more effective intercalation of CSA within the graphite galleries. Then, the collected material (see experimental section for details) was re-dispersed in *N*-methyl pyrolidone and tip sonicated until homogenized. The solution left for a

week to stand and the collected upper part of the supernatant used for functionalization with **3T** and **9T**.

The exfoliated graphene (abbreviated as **eG**) and **3T** were added in a mass ratio 2:3 in THF and the mixture was shortly sonicated and then stirred overnight resulting to a black stable solution. After that period, the mixture was centrifuged to remove any free organic material and based on consecutive sonication-centrifugation cycles any free **3T** was removed by decanting the supernatant, thus, eventually affording **3T/eG** ensemble according to Scheme 2. Following the same procedure, **9T/eG** ensemble was also acquired.

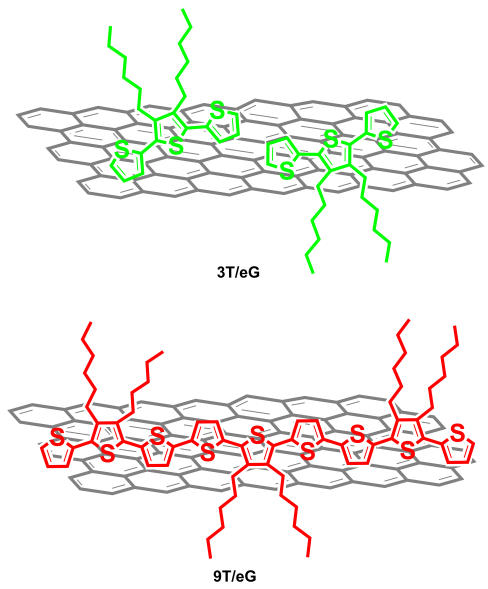

Scheme 2. Non-covalent **3T/eG** and **9T/eG** ensembles.

The quality of **eG** obtained, according to the aforementioned protocol, was evaluated by Raman spectroscopy. The samples for the measurement were prepared via drop casting of a suspension onto a 10 mm thick silicon glass and dried in vacuum at 100 ^{0}C, thus, practically measured as a thick film of the exfoliated material. In Figure 1, the Raman spectra of starting graphite and **eG**, upon laser excitation at 514 nm, are compared. Graphite possesses a characteristic Raman spectrum, comprising of the so-called G- and 2D- bands, located at 1582 and 2730 cm^{-1}, respectively. Particularly, the shape and frequency of the 2D band is sensitive to the number of graphene sheets.[34] In the Raman spectrum of **eG**, the following observations are apparent: (i) the 2D-band is almost symmetric and shifted to lower frequencies, ca. 15 cm^{-1}, as compared with the one registered from graphite, (ii) the D-band referring to defect sites, is totally missing, in accordance with intact graphite. At this point, it is interesting to note that small-sized graphene flakes, show a D-band related to edge defects,[33] thus, suggesting that our exfoliated graphene is not only of high quality lacking defects but also the applied experimental protocol did not affect, at least to great extent, the lateral size of the exfoliated graphene sheets. The Raman spectra of **3T/eG** and **9T/eG** ensembles were basically analogous to that of **eG**, with the most striking feature being the lack of an appreciable D-band, since **3T** and **9T** only supramolecularly interact with the basal plane of **eG**. In addition, for **3T/eG** and **9T/eG** the G-band was marginally shifted, ca. 2 cm^{-1}, to higher wavenumbers as compared to the one observed for **eG**, hence, indicating the occurrence of charge transfer phenomena within the nanoensembles. Furthermore, the experimentally derived 2D-band for **eG**, **3T/eG** and **9T/eG** was deconvoluted and fitted with eight, six and six Lorentzians, respectively, (ESI, Figs. S7-9). The full-width-half-maximum value for the 2D band for **eG**, **3T/eG** and **9T/eG** was calculated to be 61, 57 and 57 cm^{-1}, respectively, thereby, accordingly indicating the presence of four-, tri- and tri-layered graphene sheets.[34a, 35]

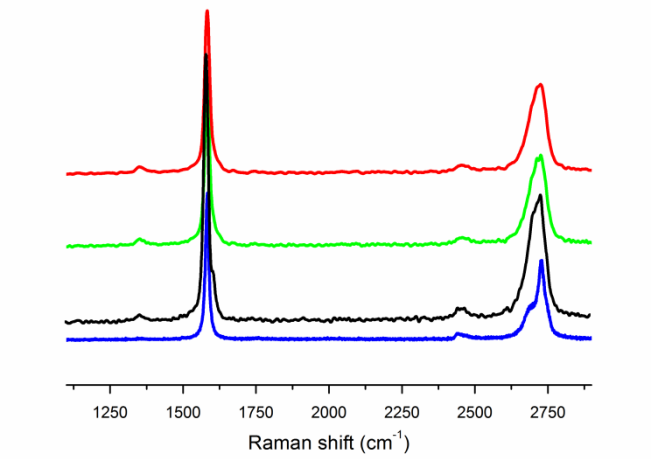

Figure 1. Raman spectra of pristine graphite (blue), **eG** (black), **3T/eG** (green) and **9T/eG** (red), obtained at 514 nm.

Notably, attenuated-total-reflectance infra-red (ATR-IR) spectroscopic studies on the **eG** revealed that it is free of oxidized species such as alcohols, epoxides, carboxylic acids or sulfonates, which demonstrates that, under the applied sonication conditions, CSA is a remarkable exfoliating agent for a wet procedure and acts exclusively as superacid, without oxidizing or sulfonating the graphene lattice (ESI, Fig. S10). As far as the ATR-IR of **3T/eG** ensemble concerns, vibrations registered for the free **3T** were discernable, namely, at 2900 cm^{-1}, due to the hexyl-chains at C-3 and C-4 and vibrations from the terthiophene backbone at the region of 600-1500 cm^{-1} (i.e. bands at 624, 824, 1077, 1216, 1373 and 1460 cm^{-1}; ESI, Fig. S11). Accordingly, in **9T/eG** ensemble, ATR-IR spectroscopy analogously verified the presence of **9T** in the ensemble by registering characteristic vibrations due to the alkyl chains at 2918 cm^{-1} as well as from the oligothiophene backbone at 1262 and 1087 cm^{-1} (ESI, Fig. S12).

High-resolution transmission electron microscopy (HR-TEM) was used to directly visualize the exfoliated graphene. Briefly, for imaging purposes, after dispersing **eG** in methanol, a drop was placed onto a copper grid and examined. Wrinkled and folded few-layered graphene sheets were identified (Fig. 2a). Even, monolayered graphene was present (Fig. 2b), as

identified according to the characteristic hexagonal pattern observed by the {1100} spots in the selected area electron diffraction and fast Fourier transformation (SAED-FFT) performed (Fig. 2c). The **3T/eG** ensemble (Fig. 2d) consists of few-layered graphene retaining the morphology of the starting graphene after supramolecularly interacting with **3T**. Similar images were registered for the **9T/eG** ensemble (Fig. 2e).

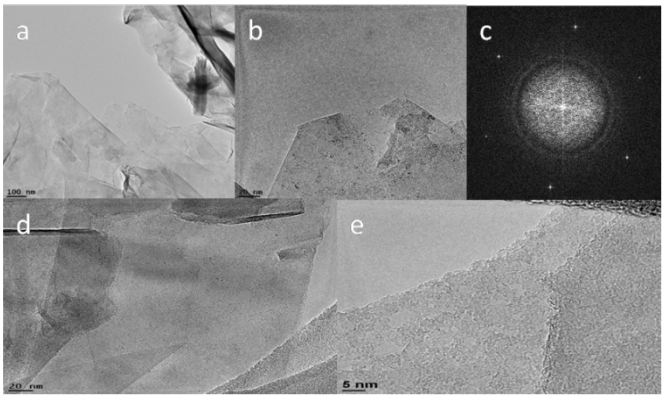

Figure 2. (a, b) Representative HR-TEM images of exfoliated graphene (**eG**), (c) SAED-FFT pattern of image shown in 2b, confirming the presence of monolayered graphene, (d) HR-TEM image of **3T/eG**, and (e) HR-TEM image of **9T/eG**.

Both **3T/eG** and **9T/eG** ensembles were found to form stable ink-like fine dispersions in THF, without observing any precipitation, hence allowing to proceed with spectroscopic studies in solution. In this frame, turning our notion to the properties evaluation, we first examined possible ground state electronic interactions between the two components of the nanoensembles. The UV-Vis-NIR spectrum of **3T/eG**, obtained in THF, showed the characteristic continuous absorption due to graphene and a broadened band centered at 327 nm corresponding to **3T**, red-shifted by 14 nm as compared to that of free **3T** (Fig. 3a). The latter red shift is related with an enhanced ability of **3T** to absorb light due to the presence of graphene as well as to a better stabilization of the hexyl-chains onto the graphene lattice.[36] Analogously, the UV-Vis absorption spectrum of **9T/eG**, obtained in THF, was characterized by a continuous absorption due to graphene and a broad oligothiophene band centered at 447 nm, red-shifted by 27 nm as compared to free **9T** (Fig. 3b). The amplification of the red shift of **9T** absorption in the **9T/eG** ensemble is in accordance with our hypothesis that the elongation of the thiophene chain and the incensement of the alkyl chains induce stronger intraensemble van der Waals forces and more effective electronic communication between the donor (**9T**) and the acceptor (**eG**) moieties.

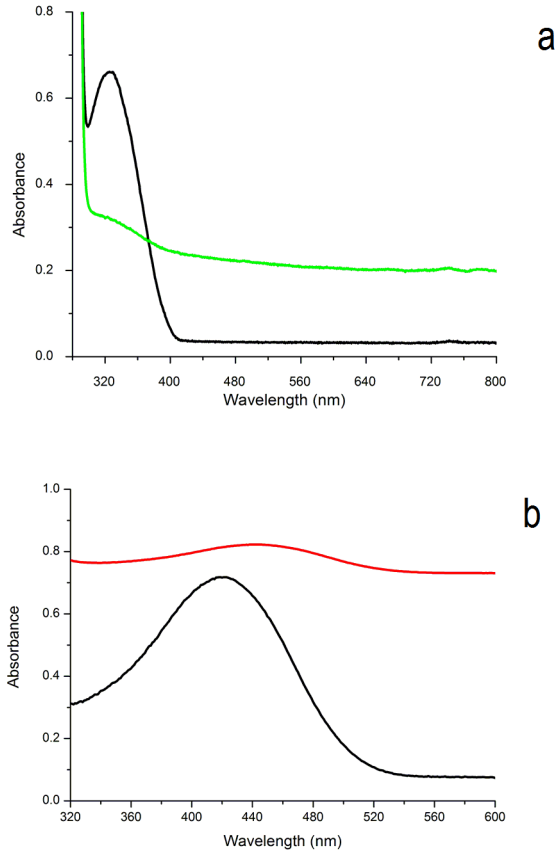

Figure 3. UV-Vis absorption spectra of a) free **3T** (black line) and **3T/eG** ensemble (green line) and b) free **9T** (black line) and **9T/eG** ensemble (red line).

Testing excited state interactions, photoluminescence assays of **3T/eG** in THF, in comparison with free **3T**, for samples possessing equal absorbance at the excitation wavelength, were performed. Photoexcitation of **3T** at 330 nm, revealed a broad emission band with maxima at 412 and 434 nm (Fig. 4a). In the **3T/eG** ensemble, the latter emission band was found quenched (Fig. 4a). Notably, when a blank sample was prepared by adding and mixing a THF solution of **3T** into well dispersed **eG** in THF (with matching absorbances at the excitation wavelength) the photoluminescence measurements conducted immediately after, revealed quenching of the **3T** emission, although not to the extent observed in the **3T/eG** ensemble. That observation, stemmed from the blank experiment, suggests that part of the emission quenching arises from the absorption of light from **eG** and part from the rapid formation of the **3T/eG** ensemble. The latter was verified when the mixture was sonicated for additional 5 min. to proceed to the formation of the ensemble and observed that the emission was further quenched (ESI, Fig. S13). Collectively, the latter result indicates strong electronic interactions between graphene and **3T** in the **3T/eG** ensemble at the excited state. Furthermore, the fluorescence quenching of the 434 nm band due to **3T** in **3T/eG** is supportive of electron

and/or energy transfer as the decay mechanism of the singlet excited state ^{1}**3T***. Then, on the basis of the time-correlated single-photon counting method, the fluorescence lifetime profiles for **3T** were acquired and scrutinized. The analysis of the time-profile of the fluorescence decay at 330 nm for ^{1}**3T*** was exclusively monoexponentially fitted, with a lifetime of 156 ps. However, measurable decay component in **3T/eG**, corresponding to the fluorescence quenching of the emission intensity in the steady-state spectra, was not observed, hence, implicitly suggesting that the singlet excited state deactivation of **3T** in the **3T/eG** ensemble is faster than the time resolution of our instrument, which is 50 ps.

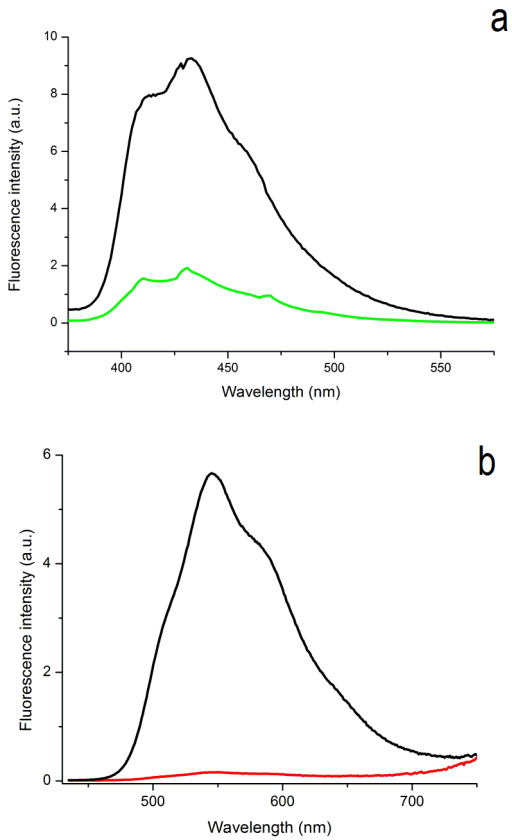

Figure 4. Fluorescence spectra of a) free **3T** (black line) and **3T/eG** ensemble (green line) and b) free **9T** (black line) and **9T/eG** ensemble (red line).

Stronger electronic interactions were revealed for the **9T/eG** ensemble. Excitation of **9T** at 420 nm resulted on a broad emission band at 545 nm, deconvoluted into two bands centered at 510 and 587 nm, which were quenched over 98% by the presence of graphene in **9T/eG** ensemble (Fig. 4b). The lifetime of the ^{1}**9T*** singlet excited state, exclusively monoexponential fitted, was 700 ps, almost 4.5 times higher than that of ^{1}**3T***. Again, in **9T/eG** ensemble, the fast decay component corresponding to the fluorescence quenching of the emission intensity was limited due to the 50 ps resolution of our instrument.

The redox data for **3T/eG** and **9T/eG** ensembles together with those for free **3T** and **9T**, versus ferrocene/ferrocenium (Fc/Fc^+ 0.33 V) in THF are presented in Table 1. At this point, it should be mentioned that unsubstituted thiophenes and oligothiophenes suffer from electropolymerization under continuous current flow, which can be a major drawback in cyclic voltammetry (CV) measurements.[37] For this reason, CV experiments were performed for a maximum of three cycles. The CV of **3T** in CH_2Cl_2 with $TBAPF_6$ as electrolyte, reveals two reversible one-electron oxidations at $E_{1/2}$ +0.47 V and +0.81 V, analogously to other oligothiophenes with comparable chain-length.[21] On the other hand, the CV graph of **3T/eG** consists of two one-electron oxidations due to the oligothiophene moiety at +0.69 V and +0.96 V, cathodically shifted by 220 mV and 150 mV as compared to the values for free **3T**, respectively. Additionally, a weak and broad reduction at -0.42 V, with current intensity of around 0.1 μA, roughly one fifth of the current of the first oxidation of **3T**, due to exfoliated graphene (ESI, Fig. S14) was observed, similarly with other reports.[9-11, 14] Notably, regarding the two oxidations in **3T/eG**, the second one is reversible, while the first one is quasi-reversible (i.e. the reduction corresponding to the first oxidation is hidden in the curve located at ~600 mV, where lies a curve observed when scanning from positive to negative potentials and the current decreases at that point), contrary to free **3T** showing both ones reversible. Based on these redox data, the formation of a radical ion pair that includes one-electron oxidation of **3T** and one-electron reduction of **eG** within **3T/eG** is possible. The electrochemical band gap for **3T/eG** ensemble is calculated to be 1.11 eV. Then, the negative free-energy change for the charge-separated state ΔG_{CS} of **3T/eG** via the singlet excited state of **3T** is evaluated as –2.06 eV by employing an energy of 3.17 eV for the singlet excited state of **3T** obtained from the crossing point of the corresponding absorption and emission spectra (ESI, Fig. S15), hence, demonstrating the thermodynamically favorable exothermic formation of the charge-separated state in **3T/eG**.

On the other hand, **9T** was easier to oxidize,[21] showing two reversible one-electron oxidations at $E_{1/2}$ +0.09 V and +0.26 V (ESI, Fig. S16). The CV of **9T/eG** reveals an anodic shift of the **9T** oxidations by 30 mV for the first oxidation and 50 mV for the second one, while both oxidations being reversible. These findings demonstrate that in the presence of graphene sheets the oxidation of **9T** becomes easier. The reduction at -0.35 V corresponds to the few-layer graphene. The electrochemical band-gap of **9T/eG** was calculated to be 0.41 eV and the energy of the singlet excited state of **9T** was calculated to be 4.0 eV from the crossing point of absorbance and emission spectra (ESI, Fig. S17). From these energy values, the ΔG_{CS} was evaluated to be -3.59 eV. Since α-unsubstituted oligothiophenes can be readily electropolymerized during continuous recording of CV, **9T** was found to be more reactive upon electropolymerization (both in solution and in the 9T/eG ensemble) probably due to the extended thiophene-backbone. This could effectively stabilize the generated charges evolved.

Table 1. Fluorescence lifetime τ_f, absorption and emission values and redox potentials for free **3T** and **9T** as well as **3T/eG** and **9T/eG** ensembles.

	Photophysical Properties			Redox Potentials (V)[b]		
	τ_f/ns	*Abs*/nm	*Emi*/nm	E_{red}	E^1_{ox}	E^2_{ox}
3T	0.10	313	412 434	-	0.47	0.81
3T/eG	≤ 0.05	327	412 434[c]	-0.42	0.69	0.96
9T	0.70	420	510 587	-	0.09	0.26
9T/eG	≤ 0.05	447	510 587[c]	-0.35	0.03	0.20

[a] in THF; [b] cyclic voltammetric studies were performed using a standard three-electrode cell. Glassy carbon was used as a working electrode and platinum wires were used as counter and pseudo-reference electrodes in 0.1 M $TBAPF_6$ in CH_2Cl_2 at 100 mV/s. $E_{1/2}$ values are shown in volts versus Fc/Fc^+; [c] broadened and quenched as compared with the emission of free **3T** and **9T**.

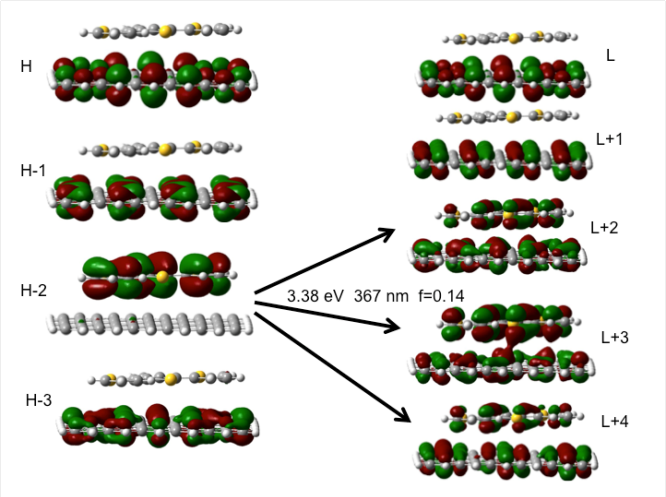

Figure 5. Illustration of the molecular orbitals involved in the first optical transition of **3T** in **3T/eG** ensemble (26th root at 367 nm). Arrows indicate configurations with the main coefficients that contribute to the first optical transition state.

Density Functional Theory (DFT) and Time-Dependent DFT (TDDFT) calculations were carried out on **3T** and on a 5X5 cluster of a graphene sheet with a **3T** molecule physisorbed on it representing **3T/eG** ensemble. The M062X functional,[38] appropriate for weak forces and charge transfer effects was employed, using the 6-31G(d,p) basis set offered by Gaussian 09. The TDDFT calculations for **3T** reproduced the main characteristics of the absorption spectrum, namely, a main line at 346 nm, with high oscillator strength f=0.81, red-shifted when THF as solvent was considered in the calculations, namely, at 369 nm, with the same oscillator strength. A similar trend was found in the calculated emission spectrum, namely, the emission at 404 nm, with an oscillator strength f=1.05 was red-shifted to 455 nm, with the same oscillator strength in THF). On the other hand, calculations on **3T/eG** predicted pure charge-transfer states with very small oscillator strengths at 821 nm (763 nm in THF) and 447 nm (434 nm in THF). Markedly, the state corresponding to the first optical transition for **3T** at 367 nm (372 nm in THF) was found to possess appreciable oscillator strength as compared to the aforementioned ones. In Figure 5, some of the highest occupied molecular orbitals and lowest unoccupied molecular orbitals were plotted, in order to reveal the character mixture of the unoccupied orbitals. Arrows pointing out the main configurations correspond to first optical transition state in **3T**, where in **3T/eG** ensemble the mix of **3T** to **3T** and **3T** to **eG** character is indicative of a charge-transfer contribution, thereby, leading to suppression of emission. Notably, the latter comes in full agreement with the photoluminescence spectra experimentally observed. Furthermore, geometry optimization of a 5X5 graphene cluster with physisorbed **3T** stabilized **3T/eG** at a distance between the two components of 3.45 A.

The latter corresponds to a coulomb attraction of 4.2 eV for electron-transfer processes from **3T** to **eG**. Then, applying the approximate Mulliken formula $E_{CT}=IP_D-EA_A-1/R_{DA}$, commonly employed for calculating the energy of an excited charge-transfer state with respect to the ground state, where (i) the ionization potential (IP) for **3T** calculated as 6.5 eV is the difference between the neutral **3T** and the corresponding cation, (ii) the electron affinity (EA) for our **eG** model found 3.0 eV is the difference between the anion and neutral graphene cluster, and (iii) R_{DA} is the distance between **3T** and **eG** (i.e. 3.45 A), the energy value for the charge-transfer state was found below the ground state, which is mainly due to the large coulomb attraction, $-1/R_{DA}$. The latter is an indication that a charge-transfer occurs in the ground state, in addition to charge-transfer in the excited state within **3T/eG**. Nevertheless, Mulliken's formula was not applicable for determining the energy of the excited charge-transfer state, direct TDDFT calculations support the formation of a charge-separated state, such as $\mathbf{3T^{\bullet+}/eG^{\bullet-}}$, which was experimentally verified by transient absorption spectroscopy (see below). Unfortunately, theoretical calculations for the **9T/eG** ensemble proved intolerable to converge at our level of calculation, particularly when considering that a very large graphene cluster was required to accommodate **9T** in a physisorbed cluster**.**

In order to conclude the analysis, transient absorption studies were performed. First, control compounds **3T**, **9T** and **eG** were evaluated in THF. As shown in the ESI, Fig. S18a, immediately after excitation, **3T** revealed a strong transient peak with maximum at 601 nm corresponding to the singlet-singlet transition. Ground state bleaching at 436 nm was also observed due to stimulated emission of **3T** (see Fig. 4a for fluorescence spectrum). The 601 nm peak decayed at a rate of 7.52×10^9 s^{-1} (time constant = 133 ps) with the appearance of a new peak at 470 nm due to intersystem crossing of ^{1}**3T*** producing ^{3}**3T*** (see ESI, Fig. S18b for time profiles). The time

constant for this process agreed well with the fluorescence lifetime of **3T** discussed earlier. Further, nanosecond transient absorption studies were performed to spectrally characterize ^{3}**3T***. As shown in the ESI, Fig. S18c, the transient absorption spectra revealed the presence of 470 nm peak with a broad shoulder extending until 630 nm. The ^{3}**3T*** decayed at a rate of 1.76 x 10^5 s^{-1} (see ESI, Fig. S18d for decay curve).

The femtosecond transient spectra features of **9T** in THF are shown in the ESI, Fig. S19a. Spectral bleaching in the 550 nm range due to stimulated emission and positive peak at 958 nm along with shoulder peaks at 908 and 1036 nm corresponding to the singlet excited transition of **9T** were observed. With time the singlet peak diminished in intensity with the appearance of new peaks at 702 and 752 nm corresponding to the triplet excited state of **9T**. The time profiles of the 958 and 702 nm peak, representing decay of ^{1}**9T*** and growth of ^{3}**9T*** are shown in the ESI, Fig. S19b. The 958 nm peak decayed at a rate of 1.46 x 10^9 s^{-1} (time constant = 684 ps), in agreement with the fluorescence lifetime of **9T**. Nanosecond transient spectral studies of **9T** confirmed the spectral identity as shown in the ESI, Fig. S19c. Transient peaks at 702 and 752 nm were observed. The ^{3}**9T*** decayed at an average rate of 1.07 x 10^5 s^{-1} (see ESI, Fig. S19d for decay profile).

The transient spectral features of **eG** in THF are shown in the ESI, Fig. S20. Instantaneous formation of optical phonon bands with peak minima at 737 and 1460 nm were observed. The signals recovered with a time constant of 3.12 ps. These features are similar to that reported earlier in literature.[4, 6, 13, 19] Attempts were also made to spectrally characterize the oxidation products of **3T** and **9T** by chemical or electrochemical oxidation. The results, however, were complicated perhaps due to polymerization of oligothiophene upon oxidation. Figure S21 in the ESI shows the spectral changes seen during oxidation of **9T** using nitrosonium tetrafluoroborate as a chemical oxidant. New broad peak in the region of 600-810 nm was observed corresponding to the oxidized product.

Femtosecond transient absorption spectra of **3T/eG** ensemble are shown in Fig. 6. The optical phonon peaks of graphene were fully developed in less than 1 ps. In addition, ^{1}**3T*** peak at 600 nm was clearly developed (see Fig. 6a spectrum at 1.5 ps) suggesting excitation of **3T** in the ensemble. Expectedly, the decay of ^{1}**3T*** was rapid. Decay of this peak was found to be biexponential with time constants of 71 and 687 ps, respectively (Fig. 6c). The lifetime of the long-lived component was close to the lifetime of pristine ^{1}**3T*** suggesting that it could arise from free **3T** (probably involving dissociation of **3T/eG** ensemble in solution). The short-lived component has been attributed to quenching due to charge transfer originating from ^{1}**3T*** within the **3T/eG** ensemble. The estimated rate of charge separation, k_{CS} was found to be 7.52 x 10^9 s^{-1}. The recovery of the photon bands of **eG** in the ensemble was found to be slightly faster than that observed in the case of pristine **eG** (Fig. 6d). A time constant of 2.86 ps was registered for this process.

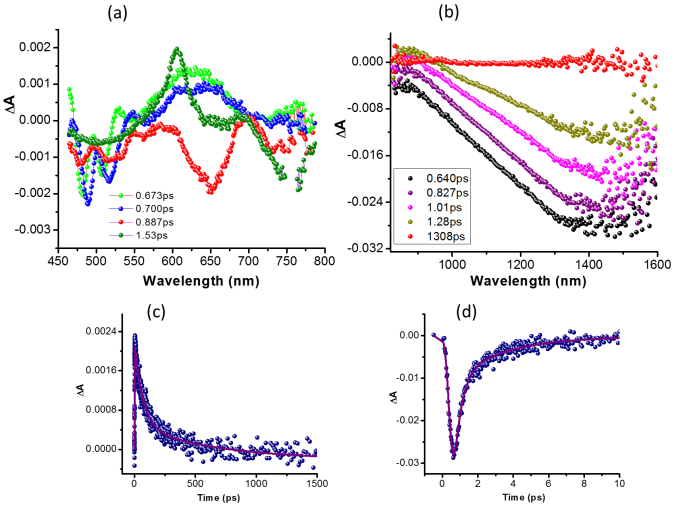

Figure 6. Femtosecond transient absorption spectra of **3T/eG** ensemble (a) in the visible and (b) near-IR regions. Time profile of the (c) 600 nm, and (d) 1450 nm, bands.

The transient spectral features of **9T/eG** ensemble, shown in Fig. 7, were also supportive of occurrence of charge separation in the ensemble. That is, immediately after excitation, phonon peaks of **eG** were observed in the visible/near-IR region in less than 1 ps in addition to broad band covering the 650-950 nm range corresponding to that of ^{1}**9T*** (see spectrum in Fig. 7a recorded at 12.4 ps). The decay of ^{1}**9T*** was also found to be biexponential with time constants of 4.5 and 781 ps, respectively. By considering the long-lived component to free **9T** and the short lived to charge separation, the k_{CS} value was estimated and found to be 2.2 x 10^{11} s^{-1}, about 30 times higher than that estimated for **3T/eG** ensemble. Debatably, the time constant for recovery of the **eG** phonon band in the **9T/eG** ensemble was shorter (2.77 ps) than that of pristine **eG** (3.12 ps) or **3T/eG** (2.86 ps). The slower k_{CS} value in **3T/eG** compared to that of **9T/eG** ensemble is comprehensible considering harder oxidation of **3T**. Also, the observed high k_{CS} value of **9T/eG** ensemble is understandable considering close association of the relatively good electron donor, **9T** on the **eG** surface, similar to the k_{CS} values reported earlier for donor/graphene hybrids.[4, 14]

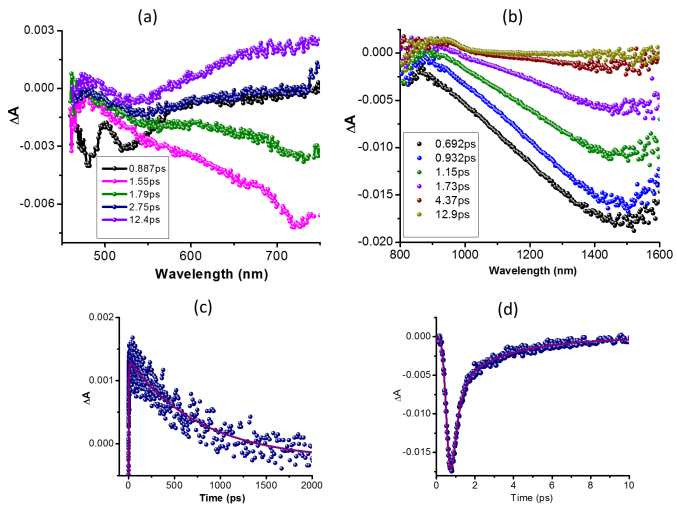

Figure 7. Femtosecond transient absorption spectra of **9T/eG** ensemble (a) in the visible and (b) near-IR regions. Time profile of the (c) 950 nm, and (d) 1450 nm, bands.

Experimental

General

All chemicals, graphite flakes and solvents were commercially available and used without further purification unless otherwise stated in supplementary information. Steady state UV-vis electronic absorption spectra were recorded on a Perkin-Elmer (Lambda 19) UV-vis-NIR spectrophotometer. Steady-state emission spectra were recorded on a Fluorolog-3 Jobin Yvon-Spex spectrofluorometer (model GL3-21). Micro-Raman scattering measurements were performed at room temperature in the backscattering geometry using a RENISHAW inVia Raman microscope equipped with a CCD camera and a Leica micro-scope. A 2400 lines mm^{-1} grating was used for all measurements, providing a spectral resolution of ± 1 cm^{-1}. As an excitation source the Ar^{+} laser (514 nm with less than 0.5 mW laser power) was used. Measurements were taken with 60s of exposure times at varying numbers of accumulations. The laser spot was focused on the sample surface using a long working distance 50C objective. Raman spectra were collected on numerous spots on the sample and recorded with a Peltier cooled CCD camera. The data were collected and analyzed with Renishaw Wire and Origin software. Electrochemical studies were performed using a standard three-electrode cell. Glassy carbon was used as a working electrode and platinum wires were used as counter and pseudo-reference electrodes (ferrocene as an internal reference). $TBAPF_6$ (98%) was recrystallized three times from acetone and dried in a vacuum at 100^0C before being used as an electrolyte. Before each experiment, the cell was purged with Ar for 30 seconds. Measurements were recorded using an EG&G Princeton Applied Research potentiostat/galvanostat Model 2273A instrument connected to a personal computer running PowerSuite software. The working electrode was cleaned before each experiment through polishing with a cloth and 6, 3 and 1 mm diamond pastes. Mid-IR spectra in the region 550–4000 cm^{-1} were obtained on an FTIR spectrometer (Equinox 55 from Bruker Optics) equipped with a single reflection diamond ATR accessory (Dura-Samp1IR II by SensIR Technologies). ^{1}H and ^{13}C NMR spectrums recorded to a Varian 300MHz spectrometer. HR-TEM measurements were carried out using a JEM-2100F (JEOL) high-resolution field-emission gun TEM operated at 80 keV at room temperature and under a pressure of 10^{-6} Pa. HR-TEM images were recorded with a charge-coupled device with an exposure time of typically 1 s.

Time-resolved fluorescence spectra were measured by a single-photon counting method using the second harmonic generation (SHG, 400 nm) of a Ti:sapphire laser (Spectra-physics, Tsunami 3950-L2S, 1.5 ps full width at half-maximum) and a streak scope (Hamamatsu Photonics, C4334-01) equipped with a polychromator (Action Research, SpectraPro 150) as an excitation source and a detector, respectively.

Femtosecond transient absorption spectroscopy experiments were performed using an Ultrafast Femtosecond Laser Source (Libra) by Coherent incorporating diode-pumped, mode locked Ti:Sapphire laser (Vitesse) and diode-pumped intra cavity doubled Nd:YLF laser (Evolution) to generate a compressed laser output of 1.45 W. For optical detection, a Helios transient absorption spectrometer coupled with femtosecond harmonics generator both provided by Ultrafast Systems LLC was used. The source for the pump and probe pulses were derived from the fundamental output of Libra (Compressed output 1.45 W, pulse width 100 fs) at a repetition rate of 1 kHz. 95% of the fundamental output of the laser was introduced into harmonic generator, which produces second and third harmonics of 400 and 267 nm besides the fundamental 800 nm for excitation, while the rest of the output was used for generation of white light continuum. In the present study, the second harmonic 400 nm excitation pump was used in all the experiments. Kinetic traces at appropriate wavelengths were assembled from the time-resolved spectral data.

The studied compounds were excited by an Opolette HE 355 LD pumped by a high energy Nd:YAG laser with second and third harmonics OPO (tuning range 410-2200 nm, pulse repetition rate 20 Hz, pulse length 7 ns) with the powers of 1.0 to 3 mJ *per* pulse. The transient absorption measurements were performed using a Proteus UV-Vis-NIR flash photolysis spectrometer (Ultrafast Systems, Sarasota, FL) with a fibre optic delivered white probe light and either a fast rise Si photodiode detector covering the 200-1000 nm range or a InGaAs photodiode detector covering 900-1600 nm range. The output from the photodiodes and a photomultiplier tube was recorded with a digitizing Tektronix oscilloscope. The transient spectral data analysis was performed using Surface Xplorer software supplied by Ultrafast Systems. All measurements were conducted in degassed THF at 298 K.

Experimental

3',4'-dihexyl-2,2':5',2''-terthiophene **(3T)**: 1 eq (0.32 mmol, 100 μL) of 2,5-di-bromo-3,4-di-hexylthiophene in dry DMF (0,32 M) and 2 eq (0.64 mmol, 204 μL) of 2-tributyl-stannyl-thiophene reacted in the presence of 2% (0.0064 mmol, 7 mg) $Pd(PPh_3)_4$,

2% (0.0064 mmol, 1.2 mg) CuI and 1 eq (0.032 mmol, 48.6 mg) CsF stirred in a sealed tube under microwave irradiation (100 W) at 120 ^{0}C for 1hr. The reaction followed by TLC with eluent petroleum ether/DCM (10:1). At that point the palladium catalyst was decomposed and black metal palladium was precipitated. The resulting mixture filtered through Celite pad and washed with petroleum ether. The DMF phase separated from the petroleum ether's phase and washed once with petroleum ether. The combined ethereal phases dried over anhydrous magnesium sulfate and evaporated to dryness. The resulting yellow oil was purified by flash column chromatography with petroleum ether as eluent to separate it from traces due to the decomposed palladium catalyst. The structure of the pure terthiophene was confirmed by ^{1}H and ^{13}C NMR spectroscopy (with TMS as a reference) and mass spectroscopy (MS). ^{1}H NMR (300 MHz, $CDCl_3$): δ = 7.35 (m, 2H), 7.13 (m, 2H), 7.06 (m, 2H), 2.69 (m, 4H), 1.54 (m, 4H), 1.33 (m, 12H) and 0.88 (m, 6H) ppm; ^{13}C NMR (75 MHz, $CDCl_3$): δ = 14.42, 22.98, 28.50, 29.94, 31.10, 31.86, 125.62, 126.20, 127.66, 130.17, 136.61 and 140.45 ppm. MS: *m/z* calculated for [$C_{24}H_{32}S_3$ +1] 417.17; found 417.30.

Tributyl(3',4'-dihexyl-[2,2':5',2''-terthiophen]-5-yl)stannane **(3)**: Initially, 1 eq of **3T** (480 mg, 1.15 mmol) dissolved in 10 mL of dry THF and cooled to -80 ^{0}C under nitrogen atmosphere. Then, 1.2 eq of BuLi (2.5M in hexanes) was added dropwise to the solution and left under stirring for 30 minutes below -50 ^{O}C. Then, 1.2 eq of Bu_3SnCl dissolved in 3 mL of dry THF was added dropwise to the mixture at -80 ^{0}C and the reaction mixture was slowly cooled down until room temperature. The reaction was quenched with petroleum ether and saturated aqueous solution of ammonium chloride. The phases were seperated, the organic phase was collected and washed with water and brine and finally dried over magnesium sulfate and vacum distilled. The crude product was purified by flash column chromatography with petroleum ether as eluent to afford the stannylated-**3T** as a light yellow oil. ^{1}H NMR (300 MHz, $CDCl_3$): δ = 7.33 (d, 1H), 7.24 (d, 2H), 7.09 (d, 2H), 2.71 (m, 4H), 1.54 (m, 10H), 1.33 (m, 24H), 0.88 (m, 6H) and 0.80 (m, 9H) ppm.

5,5''-dibromo-3',4'-dihexyl-2,2':5',2''-terthiophene **(4)**: Initially, 1 eq of **3T** (310 mg, 0.74 mmol) was dissolved in 5 mL of dry THF and cooled to -80 ^{0}C, in the abcence of light, under nitrogen atmosphere. Then, 2.5 eq of NBS was added in one portion and the mixture allowed to warm slowly to room temperature and left under stirring overnight. The organic mixture was washed three times with distilled water. The organic phase was dried over magnesium sulfate, vacuum distilled and purified by flash column chromatography with petroleum ether as eluent, affording an orange-red high viscous oil. ^{1}H NMR (300 MHz, $CDCl_3$): δ = 7.05 (d, 2H), 6.85 (d, 2H), 2.53 (m, 4H), 1.51 (m, 4H), 1.30 (m, 12H), 0.86 (m, 6H) ppm.

2, 2'- di-(*3',4'-dihexyl-2,2':5',2''-terthiophene)- 3',4'-dihexyl-2,2':5',2''-terthiophene* **(9T)**: For the synthesis of oligothiophene **9T** the same procedure followed for the synthesis of **3T** was utilized using 1 eq of **4** and 2.5 eq of **3**. ^{1}H NMR (300 MHz, $CDCl_3$): δ = 7.13 (m, 2H), 7.10 (m, 6H), 7.06 (m, 6H), 2.72 (m, 12H), 1.60 (m, 12H) 1.31 (m, 36H) and 0.86 (m, 18H) ppm; ^{13}C NMR (75 MHz, $CDCl_3$): δ = 151.66, 140.25, 135.63, 132.71, 127.34, 126.34, 125.88, 125.35, 124.86, 123.8, 38.06, 34.27, 31.92, 31.50, 30.72, 30.36, 29.69, 29.59, 28.25, 22.62 and 14.09 ppm. HR-MS: *m/z* calculated for [$C_{24}H_{32}S_3$+1] 1245.4758; found 1245.4768.

Exfoliated graphene **(eG)**: A mixture of 100 mg graphite flakes (>75%, >150 mesh) in 50 mL chlorosulfonic acid was sonicated for 8 hours. During the sonication time the temperature annealed from 30 ^{0}C to 52 ^{0}C. The resulted black homogenous solution quenched carefully (highly exothermic reaction) with distilled water. The mixture filtered through a PTFE membrane filter (pore size 0.1 μm), washed with water, methanol and dichloromethane. The filter cake was re-dispersed in NMP with the aid of bath sonication to give a black suspension. Then, the mixture was tip-sonicated (10% power) for 30 minutes and the black suspension formed was left to stand for a week at room temperature. The 2/3 of the black supernatant collected, filtered through a PTFE membrane filter (pore size 0.1 μm) and washed with water, methanol and dichloromethane.

***3T/eG** and **9T/eG** ensembles*: Exfoliated graphene (2 mg) and **3T** or **9T** (3 mg), respectively, were added in THF (5 mL), the mixture was sonicated for 5 minutes resulting in a black suspension and then stirred overnight. After that period of time, the mixture was centrifuged for 5 minutes at 4,000 rpm and the supernatant containing free **3T** or **9T**, respectively, was decanted. The centrifugation process was repeated until the supernatant was free of **3T**, or **9T**, respectively, as checked by UV-Vis spectroscopy.

Conclusions

The chrorosulfonic acid mediated exfoliation process of graphite was modified to acquire higher yield of exfoliated graphene, which was then non-covalently functionalized with the custom-synthesized oligothiophenes **3T** and **9T**, furnishing the corresponding **3T/eG** and **9T/eG** ensembles. The latter showed enhanced solubility in common organic solvents and were thoroughly characterized with standard spectroscopic and microscopy techniques. Particularly, HR-TEM imaging together with SAED-FFT verified the presence of monolayered graphene sheets. Optical studies delivered meaningful insight regarding electronic interactions between the two components within the **3T/eG** and **9T/eG** ensembles, in the ground and excited states. Particularly, there was a red-shift of the characteristic absorption band of **3T** and **9T** in the UV-Vis spectra of **3T/eG** and **9T/eG**, respectively, while importantly, efficient quenching of the emission of **3T** in the **3T/eG**, and even greater of **9T** in **9T/eG** suggests the presence of intra-hybrid electronic interactions in the excited states. Evidently, the measured fluorescence lifetimes were below the time resolution of our instrumentation, being 50 ps, suggesting

occurrence of ultrafast photoinduced processes both in **3T/eG** and **9T/eG**. Redox assays revealed the one-electron oxidation of **3T** accompanied by one-electron reduction due to **eG** in the **3T/eG** ensemble, and the two reversible one-electron oxidations of **9T** accompanied by one-electron reduction of **eG** in the **9T/eG**. The electrochemical band gap for **3T/eG** and **9T/eG** ensembles were calculated to be 1.11 and 0.41 eV respectively. The estimated free-energy change for the charge-separated state of **3T/eG** and **9T/eG** via the corresponding singlet excited state oligothiophene (^{1}**3T*** and ^{1}**9T***) were exothermic, revealing thermodynamic feasibility of such process in the ensembles. The femtosecond transient spectroscopic studies were supportive of occurrence of charge transfer type interactions in the **3T/eG** and **9T/eG** ensembles from the singlet excited oligothiophene entities. The estimated rates for photoinduced charge separation were found to be 9.52 x 10^9 s^{-1} and 2.2 x 10^{11} s^{-1}, respectively, for **3T/eG** and **9T/eG** ensembles in THF revealing modest to ultrafast photoinduced events. It is highly anticipated that more advanced ensembles incorporating oligothiophene analogues onto graphene sheets will be produced and their properties will be scrutinized and optimized for efficiently managing the charge-transfer processes and targeting photovoltaic applications.

Acknowledgements

Financial support from GSRT/NSRF 2007-2013 through action ARISTEIA II project FUNGRAPH (3150) "Functionalization of graphene with multichromophoric arrays of photoactive units for energy conversion" to NT is acknowledged. This work is also financially supported by the US-National Science Foundation (Grant No. 1401188 to FD).

Notes and references

1 A. K. Geim, K. S. Novoselov, *Nat. Mater.* 2007, **6**, 183.
2 A. Stergiou, G. Pagona, N. Tagmatarchis, *Beilstein J. Nanotechnol.* 2014, **5**, 1580.
3 a) S. P. Economopoulos, N. Tagmatarchis, *Chem.-Eur. J.* 2013, **19**, 12930; b) V. Georgakilas, M. Otyepka, B. Bourlinos, V. Chandra, N. Kim, K. C. Kemp, P. Hobza, R. Zboril, K. S. Kim, *Chem. Rev.* 2012, **112**, 6156.
4 K. Dirian, M. ´Angeles Herranz, G. Katsukis, J. Malig, L. Rodriguez-Perez, C. Romero-Nieto, V. Strauss, N. Martin, D. M. Guldi, *Chem. Sci.* 2013, **4**, 4335.
5 X. Zhang, L. Hou, A. Cnossen, A. C. Coleman, O. Ivashenko, P. Rudolf, B. J. van Wees, W. R. Browne, B. L. Feringa, *Chem.-Eur. J.* 2011, **17**, 8957.
6 M. E. Ragoussi, J. Malig, G. Katsukis, B. Butz, E. Spiecker, G. de la Torre, T. Torres, D. M. Guldi, *Angew. Chem. Int. Ed*. 2012, **51**, 6421.
7 B. Xiao, X. Wang, H. Huang, M. Zhu, P. Yang, Y. Wang, Y. Du, *J. Phys. Chem. C* 2013, **117**, 21303.
8 S. P. Economopoulos, G. Rotas, Y. Miyata, H. Shinohara, N. Tagmatarchis, *ACS Nano* 2010, **4**, 7499.
9 N. Karousis, J. Ortiz, K. Ohkudo, T. Hasobe, S. Fukuzumi, A. Sastre-Santos, N. Tagmatarchis, *J. Phys. Chem. C* 2012, **116**, 20564.
10 M. E Ragoussi, G. Katsukis, A. Roth, J. Malig, G. de la Torre, D. M. Guldi, T. Torres, *J. Am. Chem. Soc.* 2014, **136**, 4593.
11 J. Mann, J. Rodríguez-López, H. Abruňa W. Dichtel, *J. Am. Chem. Soc.* 2011, **133**, 17614.
12 N. Kozhemyakina, J. Englert, G. Yang, E. Spiecker, C. Schmidt, F. Hauke, A. Hirsch, Adv. Mater. 2010, **22**, 5483.
13 a) D. Kiessling, R. D. Costa, G. Katsukis, J. Malig, F. Lodermeyer, S. Feihl, A. Roth, L. Wibmer, M. Kehrer, M. Volland, P. Wagner, G. G. Wallace, D. L. Officer, D. M. Guldi, *Chem. Sci.* 2013, **4**, 3085; b) J. Malig, C. Romero-Nieto, N. Jux, D. Guldi, *Adv. Mater.* 2012, **24**, 800; c) J. Malig, A. W. Stephenson, P. Wagner, G. G. Wallace, D. L. Officer, D. M. Guldi, *Chem. Commun.* 2012, **48**, 8745; d) J. Geng, B.-S. Kong, S. B. Yang, H.-T. Jung, *Chem. Commun.* 2010, **46**, 5091.
14 C. Bikram, S. K. Das, K. Ohkubo, S. Fukuzumi, F. D'Souza, *Chem. Commun.* 2012, **48**, 11859.
15 A. Wojcik, P. V. Kamat, *ACS Nano* 2010, **4**, 6697.
16 J. Malig, R. Jux, D. Kiessling, J. J. Cid, P. Vásquez, T. Torres, D. Guldi, *Angew. Chem. Int. Ed*. 2011, **50**, 3561.
17 M. Kim, N. S. Safron, C. Huang, M. S. Arnold, P. Gopalan, *Nano Lett.* 2012, **12**, 182.
18 H. S. S. Ramakrishna Matte, K. S. Subrahmanyam, K. Venkata Rao, S. J. George, C. N. R. Rao, *Chem. Phys. Lett.* 2011, **506**, 260.
19 C. B. KC, G. N. Lim, F. D'Souza, *Angew. Chem. Int. Ed*. 2015, **54**, 5088.
20 A. C. Arias, J. D. MacKenzie, I. McCulloch, J. Rivnay, A. Salleo, *Chem. Rev*. 2010, **110**, 3.
21 Z. Bao, A. Dodabalapur, A. J. Lovinger, *Appl. Phys. Lett.*, 1996, **69**, 4108.
22 a) M. S. Vollmer, F. Würthner, F. Effenberger, P. Emele, D. U. Meyer, T. Stümpfig, H. Port, H. C. Wolf, *Chem.-Eur. J.* 1998, **4**, 260; b) H. Kanato, K. Takimiya, T. Otsubo, Y. Aso, T. Nakamura, Y. Araki, O. Ito, *J. Org. Chem.* 2004, **69**, 7183.
23 T.-P. Huynh, P. S. Sharma, M. Sosnowska, F. D'Souza, W. Kutner, *Prog. Polym. Sci*. 2015, in press. http://dx.doi.org/10.1016/j.progpolymsci.2015.04.009.
24 G. Barbarella, M. Melucci, G. Sotgiu, *Adv. Mater.* 2005, **17**, 1581.
25 J. M. Tour, *Chem. Rev*. 1996, **96**, 537.
26 A. Mishra, C.-Q. Ma, J. L. Segura, P. Bäurle in *Handbook of Thiophene-Based Materials*, (Eds.: I. Perepichka, D. Perepichka), Wiley-VCH, United Kingdom, 2009.
27 a) W. Domagala, M. Lapkowski, S. Guillerez, Bidan, *Electrochim. Acta* 2003, **48**, 2379; b) Z. Zak, M. Lapkowski, S. Guillerez, G. Bidan, *Synth. Met.* 2005, **152**, 185.
28 B. Capozzi, E. J. Dell, T. C. Berkelbach, D. R. Reichman, L. Venkataraman, L. M. Campos, *J. Am. Chem. Soc*. 2014, **136**, 10486.
29 R. Shokri, M.-A. Agnés Lacour, T. Jarrosson, J.-P. Lère-Porte, F. Serein-Spirau, K. Miqueu, J.-M. Sotiropoulos, F. Vonau, D. Aubel, M. Cranney, G. Reiter, L. Simon, *J. Am. Chem. Soc.* 2013, **135**, 5693.
30 X. Sun, J. Zhang, X. Wang, C. Zhang, P. Hu, Y. Mu, X. Wan, Z. Guo, S. Sei, *Chem. Commun.* 2013, **49**, 10317.
31 B. Carsten, F. He, H. J. Son, T. Xu, L. Yu, *Chem. Rev.* 2011, **111**, 1493.
32 D. H. Kim, H. S. Lee, H.-J. Shin, Y.-S. Bae, K.-H. Lee, S.-W. Kim, D. Choi, J.-Y. Choi, *Soft Mater*. 2013, **9**, 5355.
33 N. Behabtu, J.-R. Lomeda, M. J. Green, A. L. Higginbotham, A. Sinitskii, D. V. Kosynkin, D. Tsentalovich, A. Nicholas, G. Parra-Vasquez, J. Schmidt, E. Kesselman, Y. Cohen, Y. Talmon, J. M. Tour, M. Pasquali, *Nat. Nanotech*. 2010, **5**, 406.
34 a) A. C. Ferrari, J. C. Meyer, V. Scardaci, C. Casiraghi, M. Lazzeri, F. Mauri, S. Piscanec, D. Jiang, K. S. Novoselov, S. Roth and A. K. Geim, *Phys. Rev. Lett.* 2006, **97**, 187401; b) A. Gupta, G. Chen, P. Joshi, S. Tadigadapa, P. C. Eklund, *NanoLett*. 2006, **6**, 2667.
35 a) Y. Hao, Y. Wang, L. Wang, Z. Ni, Z. Wang, R. Wang, C. K. Koo, Z. Shen, J. T. L. Thong, *Small* 2010, **6**, 195; b) L. M.

Malard, M. A. Pimenta, G. Dresselhaus, M. S. Dresselhaus, *Phys. Rep*. 2009, **473**, 51.
36 T. Erb, U. Zhokhavets, G. Gobsch, S. Raleva, B. Stühn, P. Schilinski, C. Waldauf, C. J. Brabec, *Adv. Funct. Mater.* 2005, **15**, 1193.
37 Smie, A. Synowczyk, J. Heinze, R. Alle, P. Tschuncky, G. Götz, P. Bäurle, *J. Electroanal. Chem.* 1998, **452**, 87.
38 a) Y. Zhao, D. Truhlar, *Theor. Chem. Acc.* 2008, **120**, 215; b) Y. Zhao, D. Truhlar, *Acc. Chem. Res.* 2008, **41**, 157.